Noise reduction mechanisms of active noise barriers

Weisong Chen[a)], Hequn Min[b)] and Xiaojun Qiu[c)]

(Received: 24 January 2012; Revised: 10 February 2013; Accepted: 20 February 2013)

The sound field and acoustic power flow from different regions around an active noise barrier are analyzed using a two-dimensional numerical model. Results show that the noise reduction of the active noise barrier can be described as a combination of three mechanisms. They are acoustic energy transfer in space, acoustic energy absorption and radiated energy suppression by the secondary sources. At low frequencies, when the distance between the primary and secondary sources is well separated compared to the wavelength, the coupling is weak and energy reflected from the shadow zone to adjacent regions by the secondary source. Acoustic energy transfer in space is the dominant mechanism. When the primary source and the secondary source are close compared to a wavelength, the mechanisms for noise reduction can be sound absorption by the secondary source and/or the radiated power of primary source is suppressed by the secondary source. The radiated power of secondary source is negative. Furthermore, both the radiated power of primary and secondary sources fluctuates acutely with the variation of distance between them. At high frequencies, the mechanism for noise reduction can be sound absorption by the secondary source. The radiated power of secondary source is negative. © *2013 Institute of Noise Control Engineering.*

Primary subject classification: 38.2; Secondary subject classification: 31.1

1 INTRODUCTION

The mechanisms of active noise control vary with different control system configurations. According to prior work, the noise reduction mechanisms in duct and free fields are well known. In one-dimensional duct systems, when the distance between the primary and secondary sources is large compared with the wavelength, the main mechanism may be that the primary source radiated power is reflected at the location of the secondary source. However, when the secondary source is near the primary source, the main mechanism changes to that the primary source power output is suppressed by the secondary one[1,2]. If a unidirectional secondary source is used in the duct, sound power absorption is usually the dominant mechanism[3].

In three-dimensional free fields, the Kirchhoff–Helmholtz integral equation shows that the pressure in a given volume can be completely suppressed by introducing a layer of monopoles and dipoles on the surface of the volume. The mechanism may be either active absorption or reflection with continuous secondary source layer[4]. From the studies of Mangiante and Nelson et al. in free field, it is found that when the primary and secondary sources are spaced less than half wavelength, they are well coupled and the suppression of primary source power output is the dominant mechanism[5,6]. If the secondary sources are far away from the primary source, the weak coupling between these two kinds of sources causes that the secondary sources to barely affect the power output of the primary source. Therefore, the control can be the radiated power from the primary source that is absorbed or reflected by the secondary sources[7,8]. A recently developed active control methodology, difference potential method shows that the only data needed for the active control are acoustic quantities (the total sound pressure and the normal component of the particle velocity) at the perimeter of the shielded domain, and no detailed knowledge of the structure and location of the primary sources are needed. In this situation, the radiated power characteristics of primary sources and secondary sources vary with the structure of secondary sources, and the noise reduction mechanism is varied accordingly[9,10].

[a)] Anhui Normal University, Wuhu CHINA and Laboratory of Modern Acoustics of MOE, Nanjing University, Nanjing CHINA; email: weichen2711@163.com.
[b)] School of Mechanical and Aerospace Engineering, Nanyang Technological University, SINGAPORE 639798.
[c)] Laboratory of Modern Acoustics of MOE, Nanjing University, Nanjing CHINA.

Active noise barriers (ANB) has received attention since 1993, when Omoto and Fujiwara applied a multi-channel control system to cancel the noise around a semi-infinite barrier top[11]. Guo and Pan and Niu et al. claimed that canceling the sound around the barrier top had the equivalent effect of increasing the height of the noise barrier[12,13]. Han and Qiu used sound intensity as the cost function to enhance the insertion loss of the ANB system[14]. The results show that this method is more useful than other cost functions in ANB system. Recently, Hart and Lau pointed out that the method of controlling the pressure gradient on the top of the barrier is more efficient than that of controlling the sound pressure[15]. Although the above-mentioned studies on ANB systems have continued to improve the performance of the ANB systems, the noise reduction mechanisms of ANB are still not explained clearly.

A comprehensive understanding of the mechanisms of the ANB system will be beneficial for further optimization of the parameters of the system, such as locations and types of the secondary sources and the error sensors. This paper is aimed at revealing the noise reduction mechanisms of active noise barrier. Based on a two-dimensional model, the noise reduction mechanisms of the ANB system will be investigated, the sound field of the control system at different regions will be analyzed, and the radiated power of the primary and secondary sources with and without active control will be compared.

2 THEORY

To simplify the problem, the geometry of barrier, primary source row and the secondary source row can be simplified to be 2D[16,17]. In this situation, an infinite line source in the 3D space can be regarded as a "monopole" source in 2D. The two-dimensional ANB system is shown in Fig. 1, where the ground reflection is omitted to emphasize the main physics. The top of the barrier along the positive y-direction is at $(0, y_b)$ and the rigid barrier extends to infinity in the negative y-direction. A primary monopole source P is on the left side of the barrier, a secondary monopole source S is above the barrier, and N error sensors are located on the right side of the barrier. According to the principle of geometrical acoustics[18], the plane can be divided into three separated regions by the noise barrier with the dotted lines at $\pi - \theta_p$ and $\pi + \theta_p$. When the receiver is in region I, the total sound field is composed of the direct wave p_d from the primary source, the reflected wave p_r by the barrier, and the diffracted wave p_D along the edge of the barrier. When the receiver is in region II, the total sound field is composed of p_d and p_D, while for the shadow zone (region III),

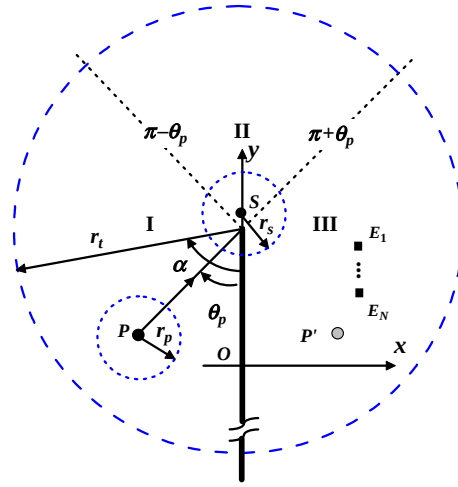

Fig. 1—Schematic diagram of a two-dimensional active noise barrier.

only the diffracted wave p_D exists. The direct and reflected waves are given by[16]

$$p_d = -\frac{j\omega\rho q_p}{4} H_0^{(2)}(kR) e^{j\omega t},$$
$$p_r = -\frac{j\omega\rho q_p}{4} H_0^{(2)}(kR') e^{j\omega t}, \quad (1)$$

where ω is the angular frequency of the sound, k is the wave number, ρ is the air density, q_p is the strength of the primary source, and $H_0^{(2)}$ is the zeroth-order Hankel function of the second kind. R and R' are respectively the distance from the receiver to the source and to its mirror image in the barrier. The diffracted wave p_D can be calculated with the Hadden and Pierce solution[17,19].

The sound pressure at the locations of N error sensors can be expressed in matrix form as[4]

$$\mathbf{p}_{\text{tot}} = \mathbf{p}_p + \mathbf{Z}_s q_s, \quad (2)$$

where $\mathbf{p}_p$ is the vector of pressure produced by the primary source at N error sensors, $\mathbf{Z}_s$ is the transfer-impedance matrix from the secondary source to the N error sensors, and q_s is the strength of the secondary source. The sum of the squared sound pressure at the error sensor positions is selected as the cost function, and the optimal strength of the secondary source is[4]

$$q_s = -\left(\mathbf{Z}_s^H \mathbf{Z}_s + \beta \mathbf{I}\right)^{-1} \mathbf{Z}_s^H \mathbf{p}_p, \quad (3)$$

where $\mathbf{I}$ is the identity matrix, β is a constraint factor for the secondary source strength, and the superscript H denotes a Hermitian transpose. Taking the top of the barrier as the center, the pressure p produced by the primary and secondary sources on a circle with radius r can be calculated according to Eqns. (2) and (3), and

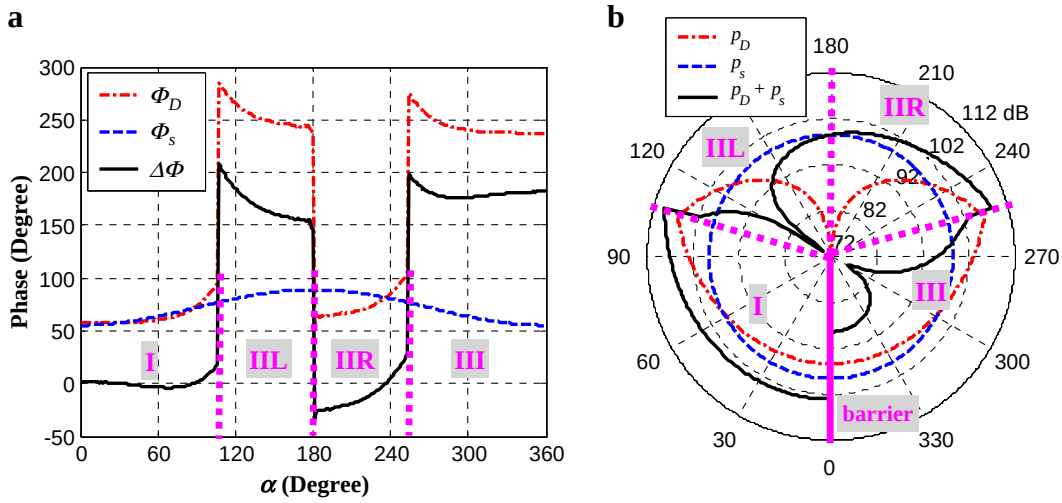

Fig. 2—(a) Phase of the pressure along a circle with radius 20 m. (b) Directivity of the pressure along a circle with radius 20 m. p_D is the diffracted wave produced by the primary source, p_s is the pressure produced by the secondary source, Φ_D is the phase of p_D, Φ_s is the phase of p_s, and $\Delta\Phi$ is the phase difference between Φ_D and Φ_s.

the radiated power can be further calculated as[4]

$$W = \frac{1}{2}\int_0^{2\pi} \mathrm{Re}[p^*(r,t)u_r(r,t)]rd\alpha, \qquad (4)$$

where α denotes the integral angle, and $u_r(r)$ is the normal velocity on the circle expressed as[4]

$$u_r(r,t) = -\frac{1}{\rho}\int \frac{\partial p(r,t)}{\partial r}dt. \qquad (5)$$

As shown in Fig. 1, the integral circle centered at the top of the barrier with a radius of r_t. The total radiated power is obtained by integrating over this circle. In the same way, the radiated power of the primary source can be obtained by integrating along a circle centered at point P with a radius of r_p, and the power radiated from the secondary source can be obtained by integrating along a circle centered at point S with a radius of r_s. The sound power flow from region II to region III can be calculated by Eqn. (4) with the integral path from the top of the barrier to infinite along the line $\alpha = \pi + \theta_p$. As the normal intensity alone the line $\alpha = \pi + \theta_p$ decreases as the distance increases between the point and the barrier top, the infinite integral in Eqn. (4) can be approximated by a finite one in practice.

3 SIMULATIONS AND ANALYSIS

As shown in Fig. 1, the barrier is rigid and the coordinates of the barrier top are (0, 1.3) m. The primary and secondary sources are at (−4, 0.1) m and (0, 1.38) m respectively, and only one error sensor is defined at (2, 0.5) m. The strength of primary source is q_p = 0.25 m^2/s with a frequency of 200 Hz. The radii r_p and r_s each equals to 2.0 m, and r_t equals to 20 m. For the calculation of the sound power flow from region II to region III, the infinite limit in the integral is substituted by 200 m along the line $\alpha = \pi + \theta_p$. The air density ρ = 1.25 kg/m^3 and the sound velocity c = 343 m/s.

3.1 The Distribution of the Sound Pressure

Figure 2(a) shows the phases of the diffraction wave p_D and the pressure of the secondary source p_s on the circle with radius r_t = 20 m, and Fig. 2(b) illustrates the directivities of p_D, p_s and the sum of the two terms. In Fig. 2(a), the phase of p_D has three π-phase jumps at $\alpha = \pi - \theta_p$, $\alpha = \pi$ and $\alpha = \pi + \theta_p$. By observing the symmetry of the sound field, the plane can be divided into four regions: region I, the left region of II ($\pi - \theta_p < \alpha \leq \pi$, abbreviated as IIL), the right region of II ($\pi < \alpha \leq \pi + \theta_p$, abbreviated as IIR) and region III.

In region III, p_D and p_s are almost out of phase, so the sum is less than p_D. In region IIL, though p_D and p_s are also almost out of phase, the large difference between their magnitudes makes the sum decrease only in the zone near $\alpha = \pi - \theta_p$. In regions I and IIR, p_D and p_s are almost in-phase, the sum of the two terms is larger than p_D alone. Therefore, the mechanism of diffraction wave reduction shows that the diffraction energy in the shadow zone is reflected to region IIR, resulting in a local quiet zone.

The directivity of the total pressure p_t on the circle with radius r_t = 20 m is shown in Fig. 3. When the control system is working, the total pressure in the shadow zone (region III) decreases significantly while the total pressure in regions I and II changes little, because the

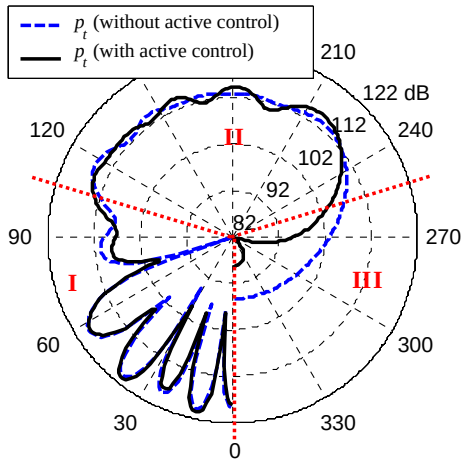

Fig. 3—Directivity of the total pressure along a circle with radius 20 m.

magnitudes of p_D and p_s are much smaller than p_d and p_r in the two regions.

3.2 The Radiated Power of the Primary and Secondary Sources

Figure 4(a) shows the radiated power of secondary source W_s as a function of the location of primary source x_p with active control at four different frequencies. Figure 4(b) gives the ratio R_{flow} of after-to-before control power which flows from region IIR to III as a function of x_p. It can be seen that all the curves in Fig. 4(a) are quasi-sinusoidal fluctuation with the variation of x_p. The fluctuation of W_s is mainly due to the interaction between the primary and secondary sources. The mutual radiation resistance of the two sources is proportional to $H_0^{(2)}$ (kr), where k is the wavenumber and r is the distance of the sources.

In low frequencies (200 or 300 Hz in Fig. 4(a)), when the primary source is far away from the secondary source, the interaction between the two sources is weak. The radiated power of secondary source is positive. The R_{flow} in Fig. 4(b) is less than 0.2. It indicates that the diffraction acoustic energy in region III is almost reflected back to region IIR after control. Therefore, energy transfer in space might be the dominant mechanism of active control. With the increasing of x_p, the distance between primary and secondary source is decreased. At several positions, the radiated power of secondary source is approaching zero, but Fig. 4(b) shows that the power flows into region III are still less than that of before control. It can be regarded as the radiation resistance of secondary source is approaching zero, but the radiation reactance is not equal to zero and it restrains the radiated power of primary source. Therefore, radiated energy suppression by the secondary source might be the dominant mechanism at these positions. As x_p increases, the interaction between primary and secondary source is enhanced. The radiated power W_s fluctuates acutely. The value of R_{flow} in Fig. 4(b) increases. The radiated power of secondary source transforms to negative for the most positions of x_p. Sound absorption of secondary source might be the dominant mechanism of active control.

For higher frequencies (500 or 800 Hz in Fig. 4(a)), the radiated power from the secondary source is negative even though the distance between primary and secondary source is large. Furthermore, the value of R_{flow} in Fig. 4(b) is larger than that at low frequencies. It means that energy transfer in space is no more the dominant mechanism of active control. However, sound absorption of the secondary source is the dominant mechanism of active control.

In order to show the detailed variation of the radiated power of primary source, Fig. 4(c) displays the ratio of after-to-before control of W_p at four different frequencies. The fluctuation of the curves reflects the interaction intensity between primary and secondary source. The lower the frequency, the more intense the interaction, when x_p is the same magnitude as the wavelength at different frequencies.

3.3 Simulation with the Finite Element Method

A commercial finite element software package COMSOL was used for the calculation of the pressure and intensity distribution[20]. All the parameters are the same as those described in Sec. 3.1. Figure 5 shows the pressure distribution and sound intensity flow without and with active control behind the barrier at 200 Hz. In order to investigate the details of the intensity, the amplitude of intensity in Fig. 5(a) larger than 0.2 w/m^2 is set to 0.2 w/m^2, and smaller than 0.08 w/m^2 is set to 0.08w/m^2. When the amplitude of intensity in Fig. 5(b) is larger than 0.02 w/m^2 it is set to 0.02 w/m^2, and smaller than 0.008 w/m^2 it is set to 0.008 w/m^2. Comparing Fig. 5(a) with 5(b), it can be seen that the pressure with active control in shadow zone decreases. In Fig. 5(b), the direction of intensity after control has changed from almost horizontal to up right in the circle zone on the left of the error sensor, which indicates that the energy is transferred to region IIR before flowing into the shadow zone.

Figure 6 shows the pressure distribution and sound intensity flow without and with active control behind the barrier at 800 Hz. Comparing Fig. 6(b) with 5(b), it shows that the direction of intensity in Fig. 6(b) changes less than that of Fig. 5(b) in the circle zone on the left of the error sensor. The result demonstrated that acoustic energy transfer in space is not the

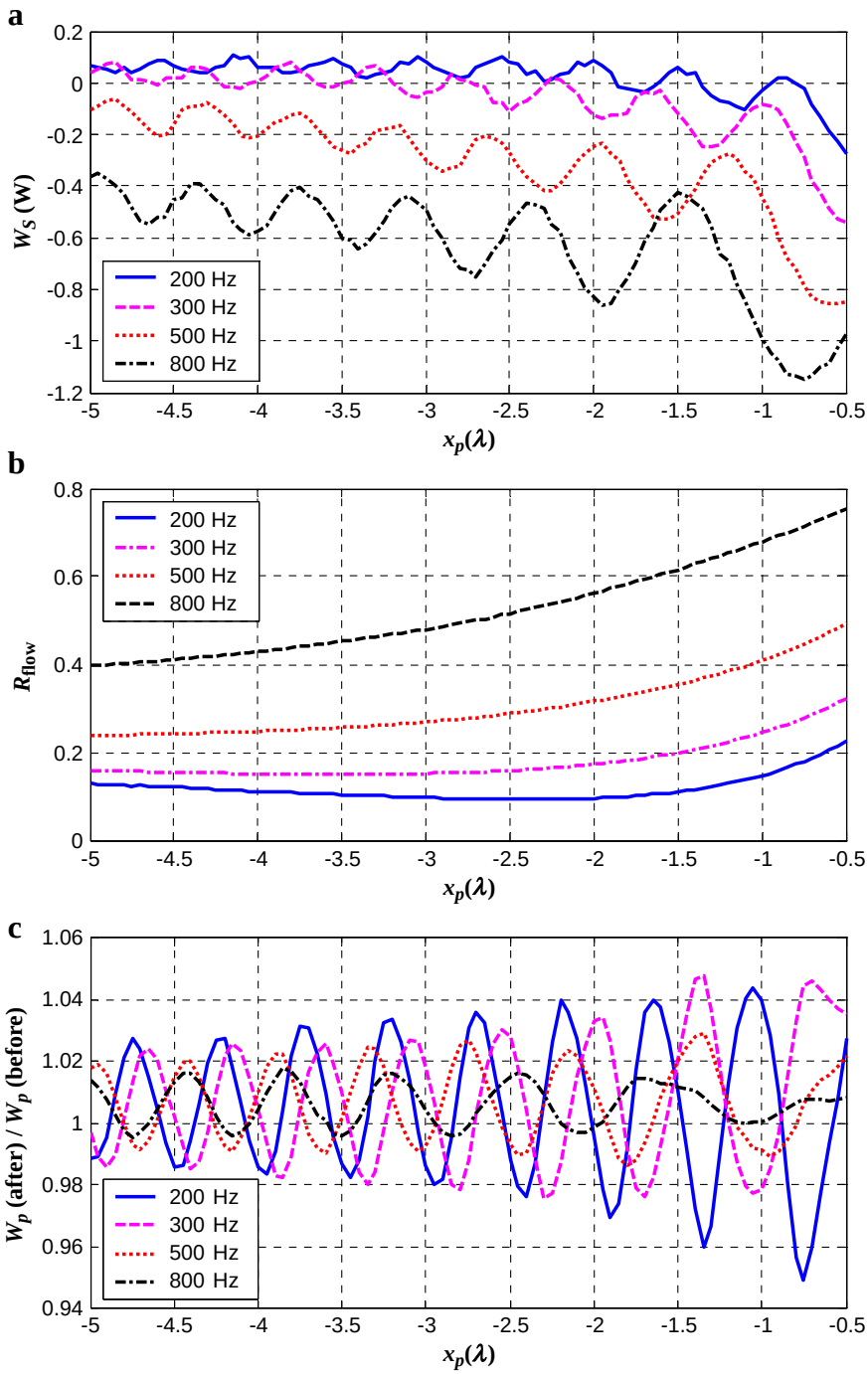

Fig. 4—The radiated power as a function of primary source location. (a) The power radiated by the secondary source. (b) The ratio of after-to-before control power which flows from region IIR to III. (c) The ratio of after-to-before control power radiated by primary source.

dominant mechanism of active control in high frequency. It might be energy absorption and/or energy suppression.

4 CONCLUSIONS

By analyzing the pressure distributions and the acoustic power flow associated with both primary and secondary sources of an ANB system, the noise reduction mechanisms of the system can be summarized as: acoustic energy transfer in the space, acoustic energy absorption and radiated energy suppression by the secondary sources.

At low frequencies, when the primary source is far from the secondary source, acoustic energy transfer in space is the dominant mechanism, and the diffraction energy in the shadow zone is reflected to adjacent region, resulting in a local quiet zone. When the distance

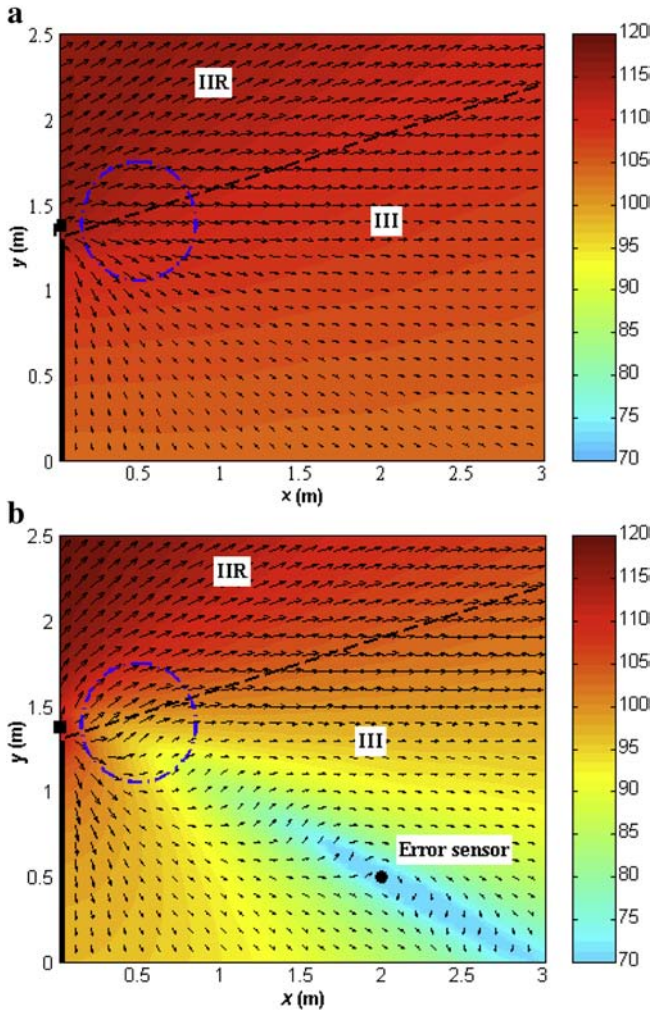

Fig. 5—Simulation results of the pressure distribution and sound intensity flow with the FEM software at 200 Hz, the unit is dB for the sound pressure and the vector arrow indicates the flow direction and magnitude of the intensity. (a) Without active control. (b) With active control.

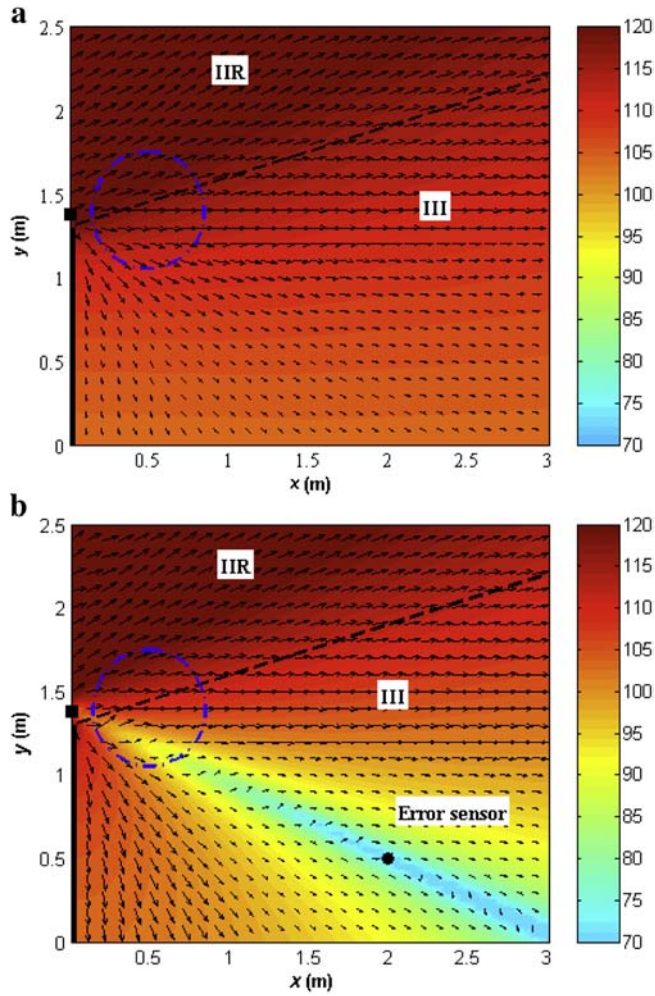

Fig. 6—Simulation results of the pressure distribution and sound intensity flow with the FEM software at 800 Hz. (a) Without active control. (b) With active control.

between the primary source and the secondary source approaches an acoustic wavelength, the energy absorption is the dominant mechanism. At high frequencies, the energy absorption is the dominant mechanism. At several specific positions, due to the interaction between the primary and secondary sources, the radiation resistance of secondary source approaches zero. However, the radiation reactance is not equal to zero and radiated energy suppression by the secondary source might be the dominant mechanism at these positions.

5 ACKNOWLEDGEMENTS

This work was supported in part by Laboratory of Modern Acoustics of MOE (Nanjing University) and Postdoctoral Science Foundation of Anhui Province. The authors would like to thank the anonymous reviewers for their constructive feedback.

6 REFERENCES

1. S. D. Snyder and C. H. Hansen, "Active noise control in ducts: Some physical insights", *J. Acoust. Soc. Am.*, **86**, 184–194, (1989).
2. J. Tian, "A theoretical explanation of the energy mechanism in active noise reduction in a duct with a monopole secondary source", *Acta Acust.*, **17**, 369–374, (in Chinese), (1992).
3. M.J.M. Jessel and G.A. Mangiante, "Active sound absorbers in an air duct", *J. Sound Vibr.*, **23**, 383–390, (1972).
4. P. A. Nelson and S. J. Elliott, *Active Control of Sound*, Academic Press, London, (1992).
5. G. A. Mangiante, "Active sound absorption", *J. Acoust. Soc. Am.*, **61**, 1516–1523, (1977).
6. P.A. Nelson, A.R.D. Curtis, S.J. Elliott and A.J. Bullmore, "The minimum power output of free field point sources and the active control of sound", *J. Sound Vibr.*, **116**, 397–414, (1987).

7. S.J. Elliott, P. Joseph, P.A. Nelson and M.E. Johnson, "Power output minimization and power absorption in the active control of sound", *J. Acoust. Soc. Am.*, **90**, 2501–2512, (1991).
8. J. Guo, J. Pan and C. Bao, "Actively created quiet zones by multiple control sources in free space", *J. Acoust. Soc. Am.*, **101**, 1492–1501, (1997).
9. J. Lončarić and S.V. Tsynkov, "Optimization of power in the problems of active control of sound", *Math. Comput. Simulation*, **65**, 323–335, (2004).
10. V.S. Ryaben'kii, S.V. Tsynkov and S.V. Utyuzhnikov, "Active control of sound with variable degree of cancellation", *J. Appl. Math. Lett.*, **22**(12), 1846–1851, (2009).
11. A. Omoto and K. Fujiwara, "A study of an actively controlled noise barrier", *J. Acoust. Soc. Am.*, **94**, 2173–2180, (1993).
12. J. Guo and J. Pan, "Increasing the insertion loss of noise barriers using an active-control system", *J. Acoust. Soc. Am.*, **104**, 3408–3416, (1998).
13. F. Niu, H.S. Zou, X.J. Qiu and M. Wu, "Error sensor location optimization for active soft edge noise barrier", *J. Sound Vibr.*, **299**, 409–417, (2007).
14. N. Han and X.J. Qiu, "A study of sound intensity control for active noise barriers", *Appl. Acoust.*, **68**, 1297–1306, (2007).
15. C.R. Hart and S.K. Lau, "Active noise control with linear control source and sensor arrays for a noise barrier", *J. Sound Vibr.*, **331**, 15–26, (2012).
16. H. Min and X. Qiu, "Multiple acoustic diffraction around rigid parallel wide barriers", *J. Acoust. Soc. Am.*, **126**(1), 179–186, (2009)
17. H.S. Kim, J.S. Kim, H.J. Kang, B.K. Kim and S.R. Kim, "Sound diffraction by multiple wedges and thin screens", *Appl. Acoust.*, **66**, 1102–1119, (2005).
18. K.M. Li and H.Y. Wong, "A review of commonly used analytical and empirical formulae for predicting sound diffracted by a thin screen", *Appl. Acoust.*, **66**, 45–76, (2005).
19. D. Ouis. "Noise attenuation by a hard wedge-shaped barrier", *J. Sound Vibr.*, **262**, 347–364, (2003).
20. Comsol Multiphysics 3.5, Last view: November 2011 (http://www. comsol. com).